

# Imaging spatio-temporal fluctuations and local susceptibility in disordered polymers

N. E. Israeloff, P. S. Crider and M. E. Majewski

Dept. of Physics, Northeastern University, Boston, MA 02115

## ABSTRACT

Spatial and temporal fluctuations of the electric polarization were imaged in polymer thin films near the glass transition using electric force microscopy. Below the glass transition the fluctuations are quasi-static and spatial fluctuations were found to quantitatively agree with predictions for thermal fluctuations. Temporal fluctuations appear near the glass transition. Images of the space-time nanoscale dynamics near the glass transition are produced and analyzed. Local, complex dielectric susceptibility was also studied, and shows that dynamics on the free-surface are faster relative to the bulk.

Glass transition, noise, polymers, fluctuations, dielectric susceptibility, complex systems

## 1. INTRODUCTION

Thermal fluctuations measured locally in complex materials can reveal important features of the microscopic dynamics;<sup>1-3</sup> Via the fluctuation-dissipation-relation (FDR), local moduli such as rheological properties can be inferred from the fluctuations<sup>4</sup>. On the other hand, local deviations from the FDR have been predicted for aging glassy systems<sup>5</sup>. Recent theory of glasses has also emphasized space-time trajectories of the spontaneous dynamics<sup>6-8</sup>. In addition, four-point space-time correlation functions have been used to define dynamical correlation lengths, which have been seen to grow on cooling in some simulations<sup>8,9</sup>. In this paper we report on quantitatively imaging thermal fluctuations of the electric polarization<sup>10</sup>, with nano-scale resolution, near the glass transition,  $T_g$ , in thin polymer films. Spatio-temporal images of these fluctuations are produced and analyzed.

## 2. EXPERIMENTS

Electric force microscopy (EFM) is a scanning probe microscopy (SPM) method in which local electrostatic forces are probed. EFM has been used to image localized charges<sup>11</sup> on surfaces, and dielectric constant variations<sup>12</sup>. In EFM a conducting cantilever is used so that DC and AC bias voltages can be applied to the tip (nominal tip radius  $R \sim 25$ -30 nm). We use an ultra-high-vacuum SPM with a variable-temperature stage (RHK UHV 350). In vacuum, the quality-factor of the cantilever's resonance is extremely high ( $>20,000$ ), and therefore amplitude-modulation non-contact imaging (typically done in air) is not possible. Instead, a non-contact frequency-modulation (FM) imaging mode is used. In this mode, the cantilever is oscillated at its resonance-frequency,  $f_{res} \sim 70$  kHz, using a Nanosurf EasyPLL phase-locked-loop and detector system. With this setup, a frequency shift,  $\delta f_{res}$ , due to tip-sample interaction forces is detected with very high resolution, and this is used as a feedback parameter for controlling the tip-sample distance,  $z$ . The samples are thin films (thickness  $\sim 1$   $\mu\text{m}$ ) of poly-vinyl-acetate (PVAc) ( $M_w = 167,000$ ), which have been prepared by spinning from a toluene solution, onto Au on glass, and annealed near  $T_g = 308$  K for 24 hours in vacuum. The Au film forms a back electrode which is grounded. Typical dielectric susceptibility behavior was found, when measured in identically prepared bulk samples with a top (AuPd) electrode, using a Novovcontrol dielectrometer.

The electrostatic force on the SPM tip has a derivative,  $dF/dz$ , which acts to slightly reduce the effective spring constant of the cantilever (nominal  $k \sim 2$  N/m) and thereby its resonance frequency,  $f_{res}$ . Since the charging energy of the tip-sample capacitance is  $U = \frac{1}{2}CV^2$ , then the  $dF/dz = \frac{1}{2}V^2 d^2C/dz^2$ . We apply an oscillating tip bias,  $V=V_0\sin(\omega t)$ , at frequencies much lower than  $f_{res}$ . With the squaring of  $V$ , a  $2\omega$  signal appears, reduced by a trigonometric factor of  $\frac{1}{2}$ . This  $V_{2\omega}$  signal is given by:

$$V_{2\omega} = \frac{A}{4} \frac{\delta k}{k} f_{res} = \frac{A}{4k} \frac{\partial F}{\partial z} f_{res} = \frac{A}{8k} \frac{\partial^2 C}{\partial z^2} V_0^2 f_{res} \quad (1)$$

where  $A$  is a gain factor from the Nanosurf detector. The capacitance as a function of height above the surface,  $C(z)$ , can be modeled using a finite-element (Bela) calculation for a realistic tip shape (a cone with hemispheric tip of radius,  $R$ ). This calculation also gives us an effective volume probed, defined as the region over which the electric field drops a factor of two. See figure 1. From comparison with our measured  $V_{2\omega}$  vs.  $z$ , we obtain  $R=28\pm 4$  nm, consistent with cantilever specifications. And a measurement height of  $z_0=16.5\pm 1$  nm will apply for the measurements described below. The probed region has a depth of  $20\pm 5$  nm, and radius of  $25\pm 5$  nm. As described in detail elsewhere<sup>13</sup>, we have been able to use the amplitude and phase of the  $V_{2\omega}$  to measure local frequency-dependent dielectric spectroscopy.

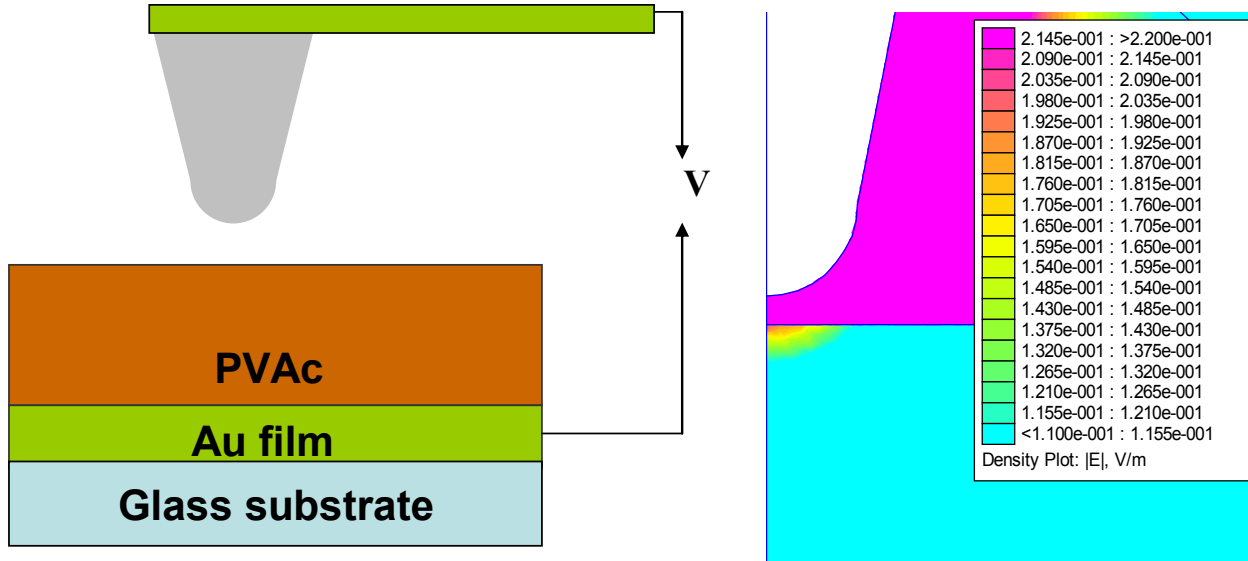


Figure 1. Measurement setup on the left, showing the conducting SPM tip and dielectric sample. On the right is a finite-element calculation, showing the electric fields dropping a factor of two in the colored region below the tip.

The voltage applied to the tip produces a charge,  $C_{tip}V$ , and an image charge in the sample,  $Q'_{tip}$ . Any polarization-induced surface potential  $V_p$  on the sample surface conversely produces an image on the tip,  $Q'_p = C_{tip}V_p$ . The total tip charge is then  $Q_{tip} = C_{tip}(V+V_p)$ . It is the Coulomb force on the tip, or rather its  $z$  derivative, that we observe in the measurements as a resonance frequency shift. Again, we can obtain it from the second derivative of charging energy  $U = \frac{1}{2} Q_{tip}^2 / C_{tip} = \frac{1}{2} C_{tip} (V+V_p)^2$ . After squaring, the cross term causes a  $1\omega$  signal to appear:

$$V_{\omega} = \frac{A}{2k} \frac{\partial^2 C}{\partial z^2} V_0 V_p f_{res} \quad (2)$$

Combining eqns. 1 and 2 we obtain a simple expression for  $V_p$  in terms of  $V_\omega$  and  $V_{2\omega}$  which can both be easily measured with a lock-in amplifier (Stanford 830):

$$V_p = V_0 V_\omega \frac{V_0 V_\omega}{4V_{2\omega}} \quad (3)$$

With the SPM software we can image any external signal, while using another signal as feedback parameter. In this case, the feedback parameter is  $\delta f_{\text{res}}$  while the imaging signal is  $V_\omega$  from the lock-in amplifier. The tip voltage is oscillated at as high a frequency as possible, which is typically 95 Hz, giving a  $2\omega$  at 190 Hz which is at the upper end of the sensitivity band of the Nanosurf detector. A filter with 25 Hz cutoff is applied to the feedback signal to limit the tip height from oscillating at  $2\omega$ .  $V_{2\omega}$  is measured before and after each image to use with eqn. 3 to obtain a polarization image.  $V_{2\omega}$  does not vary more than 5 % across the sample under fixed conditions.

In figure 2, we show a series of three polarization ( $V_p$ ) images of the same 700 nm square region of PVAc at  $T=303$  K, which is 5K below the bulk glass transition. Here the oscillating bias is 1 V rms. Note: the dynamics observed are independent of this applied voltage. The lock-in time constant was typically set to 30 ms, giving a low-pass filter with cut-off of about 5 Hz. The images show interesting, apparently random structure. This structure is reproducible over short time intervals but is quite distinct from the topography. The topography (height) was quite smooth aside from a distinct bump used as a marker. This bump appears as a dark oval in the upper left of these images. Most striking, the images show evolution with time at temperatures close to  $T_g$ . After 17 minutes, there is some similarity in the second image but considerable loss of correlation. The third image, measured 48 minutes after the first shows nearly complete loss of correlation with the initial one.

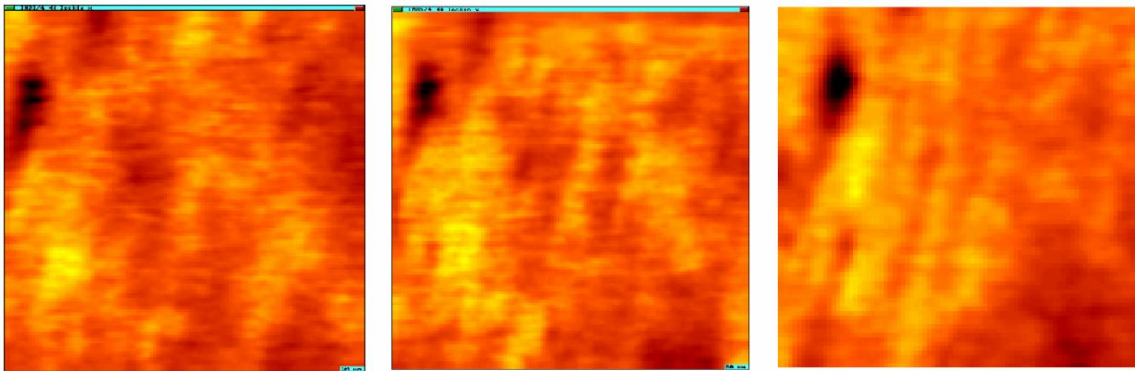


Figure 2. Polarization images (650 nm x 650 nm) of the same region in PVAc at  $T= 303$ K. The dark oval at upper left is a topographic feature used as a marker. Middle, right images were measured 17, 48 minutes after left image.

Near the glass transition of a polymer, the dielectric susceptibility,  $\epsilon$ , has a fast component,  $\epsilon_\infty$ , and a slow component due to glassy reorientation of polar molecules,  $\Delta\epsilon = \epsilon_s - \epsilon_\infty$ . The tip capacitance,  $C_{\text{tip}}$ , can thus be replaced with an equivalent circuit, in which the sample surface to back electrode forms a capacitance whose fast component we designate  $C_\infty$  and slow component (series resistor) we designate,  $C_{\Delta\epsilon}$ , and the tip to sample surface capacitance,  $C_{\text{vac}}$ . See figure 3. In this equivalent RC circuit, thermal noise generated in  $R(\omega)$  will produce an rms voltage on the equivalent capacitance,  $C_{\text{eq}}$ , in the circuit given by:

$$\delta V = \left[ \frac{k_B T}{C_{\text{eq}}} \right]^{1/2} \quad (4)$$

The voltage  $V_p$  of interest is the voltage across  $C_{\text{vac}}$ , which will be reduced to:

$$\delta V_p = \left[ \frac{k_B T}{C_{eff}} \right]^{1/2} \quad (5)$$

where  $C_{eff}$  is an effective capacitance given by:

$$C_{eff} = [C_\infty + C_{vac}] \left[ \frac{C_\infty + C_{vac}}{C_{\Delta\epsilon}} \right] \quad (6)$$

From the finite element model (FEM) we obtain  $C_{\Delta\epsilon} = 2.5 \pm 0.2 \times 10^{-18} \text{F}$ ,  $C_\infty = 5.6 \pm 0.5 \times 10^{-18} \text{F}$ ,  $C_{vac} = 1.5 \pm 0.1 \times 10^{-18} \text{F}$  giving a  $C_{eff} = 6.9 \pm 0.4 \times 10^{-18} \text{F}$ . Using equation 5 and 6 we can predict  $\delta V_p = 24.0 \pm 1 \text{ mV}$  for our measurement conditions. It is this noise that gives an observable noise in  $V_\omega$ , via eqn. 2. Note that this would be the total integrated temporal noise in one spatial location.

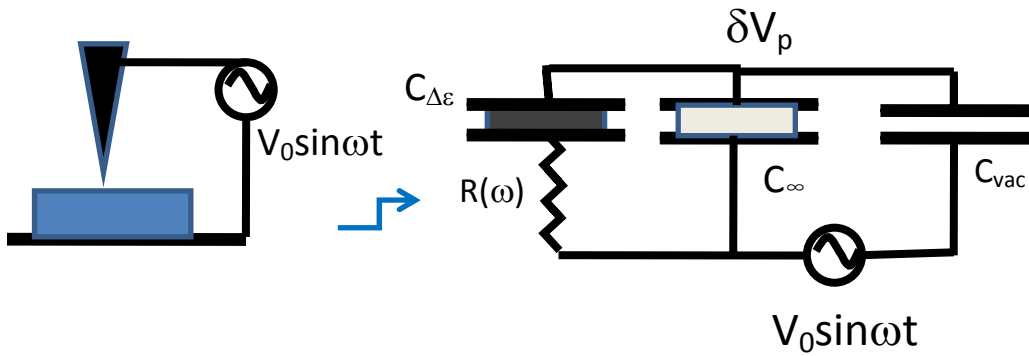


Figure 3. SPM tip above dielectric sample and equivalent circuit for noise analysis.

We can also consider this noise to be a local dipole moment fluctuation,  $\delta\mu$  in a small volume  $\Delta\Omega$ . The mean-squared local moment fluctuations will be:

$$\langle \delta\mu^2 \rangle = k_B T \Delta\chi \Delta\Omega \quad (7)$$

Here,  $\Delta\chi$  is the slow (glassy) part of the susceptibility. If we consider a small cylindrical volume of radius,  $r = 25 \text{ nm}$  and height,  $h = 20 \text{ nm}$  beneath the tip, i.e. similar in size and shape to the effective volume seen in figure 1, we find the rms moment fluctuations are  $\delta\mu \sim 3 \times 10^{-27} \text{ Cm}$ . This would produce a voltage fluctuation on the cylinder,  $\delta V = \delta\mu / \epsilon \pi r^2 \sim 27 \text{ mV}$ , using a mean value for  $\epsilon$ . This is a reassuringly similar result.

We can also consider the force and force derivative on the dipole moment fluctuation within each volumetric element and we find:

$$\frac{\partial F}{\partial z} = \frac{\partial^2 \mathbf{E}}{\partial z^2} \cdot \delta\mu \quad (8)$$

When we also add in the effect of the tip image charge, we are able to convince ourselves, at least for a parallel-plate model, that when summed up over all volume eqn. 7 and eqn. 2 are equivalent.

Equation 5 predicts the integrated temporal fluctuations in  $V_p$  that would be observed in a single location. However, by scanning, we are in essence sampling different capacitors. At temperatures just below  $T_g$ , the fluctuations are essentially frozen-in for hundreds of seconds. Thus, we expect the *spatial* variations in  $V_p$  to reflect the full variance as given by eqn. 5, for a fast enough scan. Polarization images like those in figure 2 were analyzed at two temperatures below  $T_g$ . Temperatures were selected such that complete decorrelation was observed within about an hour. The very long-time averaged ( $> 1$ hour) image was assumed to be a static background due to topography and was first subtracted to produce a  $\delta V_p$  image. The standard deviation of  $\delta V_p$  was characterized for several images at each temperature. At 303.5 K, we observed  $\langle \delta V_p \rangle = 23 \pm 4$  mV. At 305.5 K, we found  $\langle \delta V_p \rangle = 28 \pm 4$  mV. This agreement with the prediction of  $24.0 \pm 1$  mV is striking given the uncertainty in our knowledge of the tip shape.

In order to begin studying various spatial and temporal correlation functions, we wanted to first obtain images which had good resolution in both space and time. To do this we sacrifice one of the spatial dimensions. A standard x-y image is obtained by scanning rapidly in x and slowly in y. By turning off the slow scan, we repeatedly measure the same x scan line. The resulting image is an x-t scan. The time per line is typically 9 seconds. Space-time images for two temperatures are shown in figure 4. One can clearly see temporal (vertical) correlation that lengthens in time at lower temperatures. This is consistent with the fact that glassy relaxation times grow rapidly with decreasing temperature on passing through the glass transition. There are possibly hints of web-like structures in the lower temperature images.

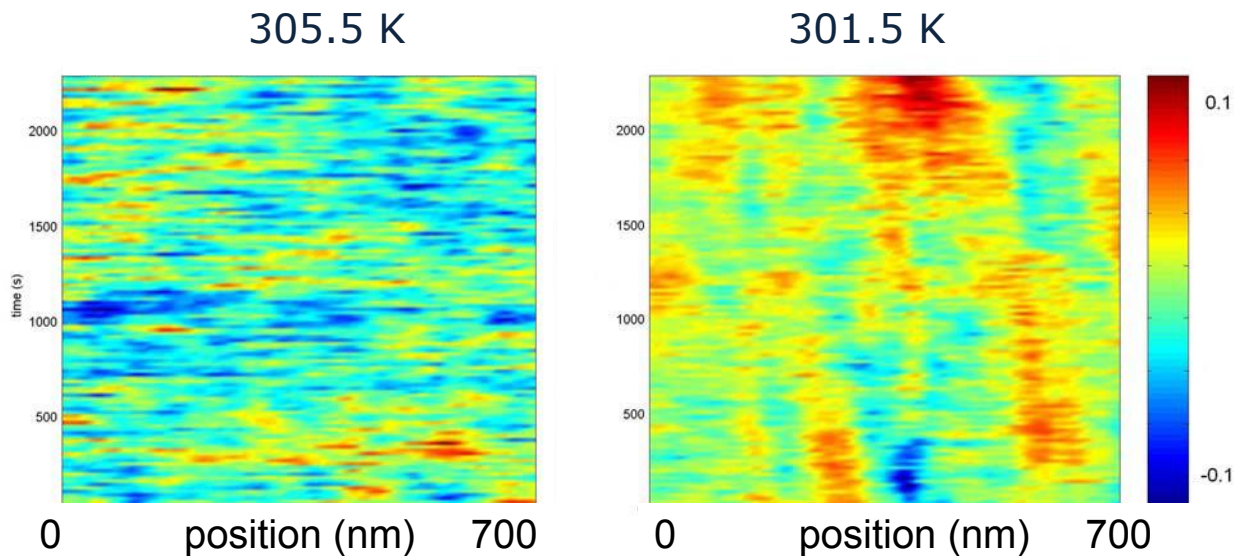


Figure 4. Polarization space-time images, 700nm x 2500 s, for the two temperatures indicated.

The space-time images offer the opportunity to study various correlation functions. The simplest being the global average time-correlation function,  $\langle C(t) \rangle$ , which reveals the overall characteristic lifetime(s) of glassy configurations. This is obtained by performing an autocorrelation at each spatial position, then averaging these over all positions. At each temperature several images like those in figure 4 are analyzed and averaged. In figure 5, we show the  $\langle C(t) \rangle$  for three temperatures. We can clearly see the increasing relaxation time for decreasing temperature, and the shape is reminiscent of the stretched-exponential bulk behavior of various correlation or relaxation functions. When we study the global average spatial correlation function, averaged over time, at least at the higher temperatures, we find a rapid decay with a characteristic length of about 25 nm. We believe this length is simply the instrumental resolution determined by the tip size and consistent with the half width of the effective volume probed (Fig. 1). We can also sit at a

single spatial location and take very long time-series. With these we can analyze with high resolution the correlation function, or do the usual noise power spectrum. In figure 6, we show the power spectrum for three temperatures, the highest of which shows the expected characteristic knee of a broadened Lorentzian, that is predicted from the Nyquist relation. We can also study the response of the polarization to applied dc or ac fields. Following a long-time application of a dc bias of 500 mV, we obtain local dielectric relaxation curves which can be averaged several times, as shown in the inset of figure 5. As might be expected, these have a similar shape to the correlation functions. By applying a low frequency (.01-100 Hz) ac bias, and studying the amplitude and phase of  $V_{2\omega}$ , we can extract the frequency-dependent complex susceptibility curves, as shown in the inset of figure 6<sup>13</sup>. As discussed in detail elsewhere, the susceptibility measurements showed that the glass transition temperature of a free surface of PVAc were shifted to lower by  $\sim 4$  K relative to bulk<sup>13</sup>. Whether in the frequency or the time domain, it should be possible to quantitatively compare the noise and response in order to test the fluctuation-dissipation-relation (FDR) in non-equilibrium.

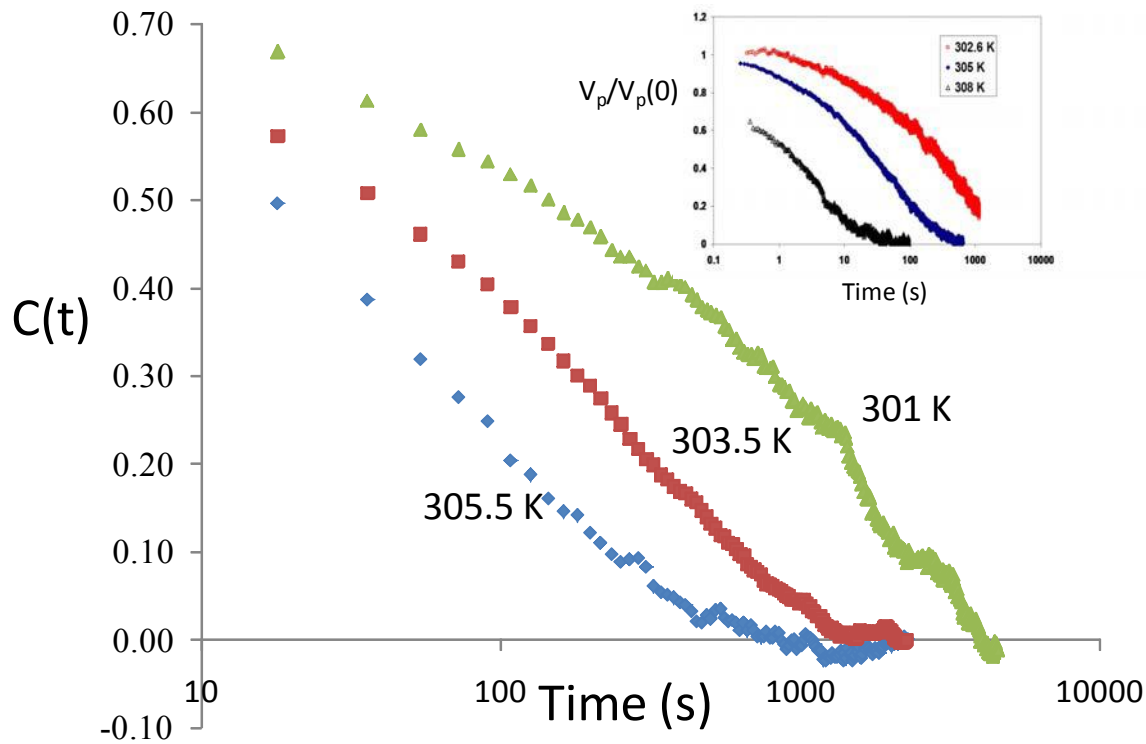


Figure 5. Global average time correlation function, obtained from x-t images like those in figure 3, for the three temperatures indicated. Inset: local normalized dielectric relaxation curves for 308K, 305K, and 302.6 K.

### 3. DISCUSSION AND CONCLUSIONS

We have described a new method for locally probing spatio-temporal fluctuations which agree quantitatively with predictions for thermal noise. This method may be useful for studying complex nanoscale dynamics such as near the glass transition in polymers or liquids. Dielectric susceptibility in the frequency<sup>13</sup> or time domain<sup>14</sup> was also measured locally. If both noise and susceptibility can be measured near simultaneously, possible violations of the FDR during aging (following a temperature quench) could be studied locally, as has been done in simulations<sup>15</sup>. We also measured the simplest global correlation functions in space-time fluctuation images. More complex correlation functions can also be studied. Various four-point space-time correlation functions have been studied in simulations. A recurring one is  $g_4(x,t) = \langle V(0,0)V(0,t)V(x,0)V(x,t) \rangle - \langle V(0,0)V(0,t) \rangle \langle V(x,0)V(x,t) \rangle$ , which is sensitive to dynamics which are correlated at a distance  $x$ . When integrated over all  $x$ , a generalized susceptibility,  $\chi_4(t)$ , is obtained. In simulations, such

as molecular dynamics simulations of Lennard-Jones glasses, this has been found to exhibit a peak at the average relaxation time. The height of the peak, which is said to be proportional to a dynamical correlation length, grows on cooling<sup>9</sup>. The only experimental studies of  $\chi_4(t)$  have been on colloidal glasses. It would be very useful to study such correlation functions in  $x, t$  images of structural glasses such as those described here. Though the correlation length is likely to be slightly less than the resolution of our measurements, the global  $\chi_4(t)$ , which can be described as the variance of the correlation function  $C(t)$ , may exhibit residual enhancement. Results of such an analysis will be reported elsewhere.

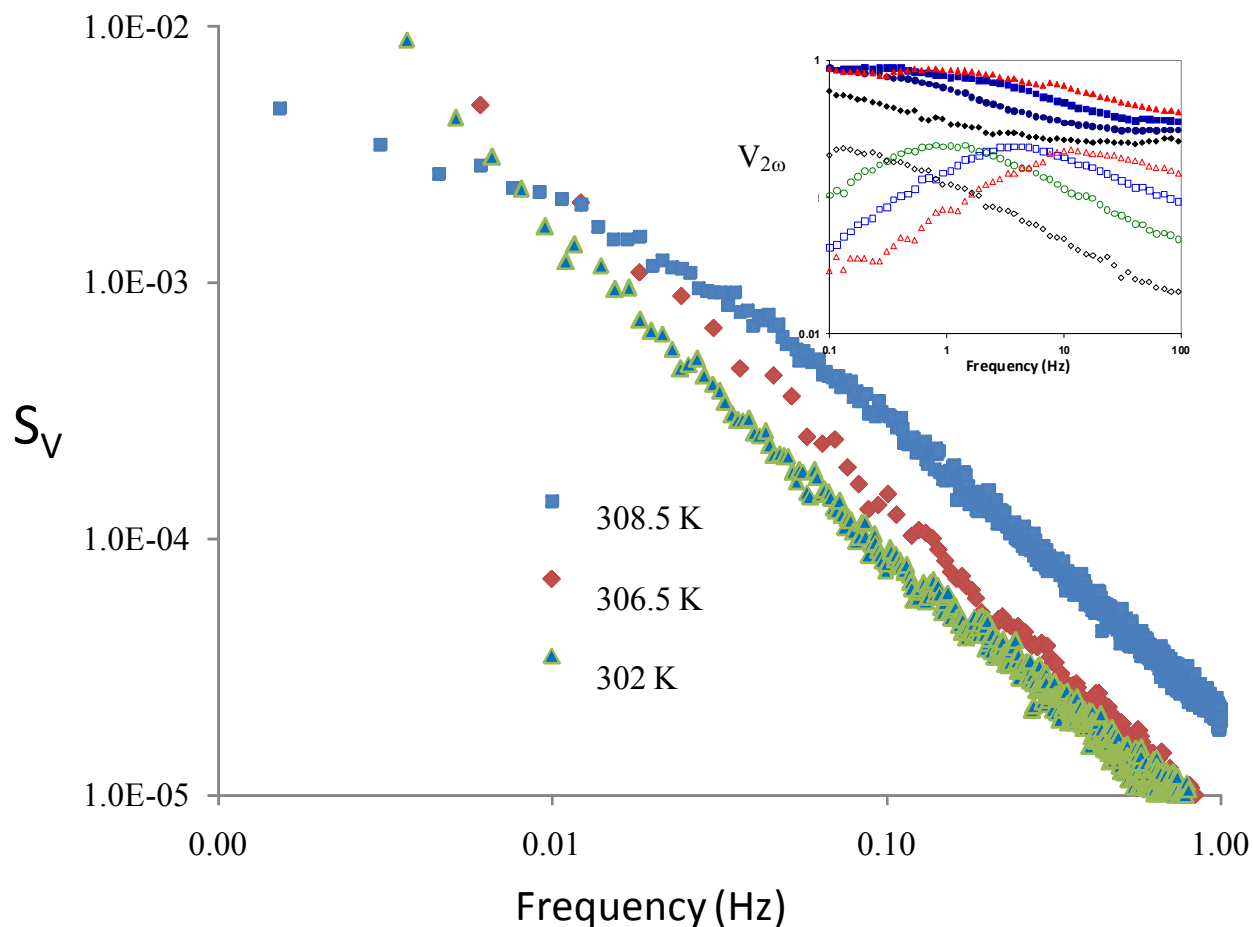


Figure 6. Polarization noise power spectra for fixed position at three temperatures. Inset: local real and imaginary components of locally measured dielectric susceptibility vs. frequency for several temperatures.

### ACKNOWLEDGEMENTS

This work was supported by NSF grant DMR-0606090 and ACS-PRF 38113-AC7. We thank Hassan Oukris and Jingyun Zhang for assistance.

### REFERENCES

1. E. R. Weeks, D. A. Weitz, J. C. Crocker, A. C. Levitt, and A. Schofield, "Properties of cage rearrangements observed near the colloidal glass transition", *Phys Rev Lett* **89**, 095704 (2002).

2. E. Vidal Russell, and N. E. Israeloff, "Direct observation of molecular cooperativity near the glass transition," *Nature* **408**, 695-698 (2000).
3. A. Berengere, and G. Francois, "Probing a Nonequilibrium Einstein Relation in an Aging Colloidal Glass," *Physical Review Letters* **93**, 160603 (2004).
4. T. G. Mason, and D. A. Weitz, "Optical measurements of frequency-dependent linear viscoelastic moduli of complex fluids," *Physical Review Letters* **74**, 1250-1253 (1995).
5. H. E. Castillo, C. Chamon, L. F. Cugliandolo, and M. P. Kennett, "Heterogeneous Aging in Spin Glasses," *Physical Review Letters* **88**, 237201-237204 (2002).
6. M. Merolle, J. P. Garrahan, and D. Chandler, "Space-time thermodynamics of the glass transition," *Proceedings of the National Academy of Sciences of the United States of America* **102**, 10837-10840 (2005).
7. D. Chandler, and J. P. Garrahan, "Thermodynamics of coarse-grained models of supercooled liquids," *The Journal of Chemical Physics* **123**, 044511 (2005).
8. J. P. Garrahan, and D. Chandler, "Geometrical Explanation and Scaling of Dynamical Heterogeneities in Glass Forming Systems," *Physical Review Letters* **89**, 035704 (2002).
9. C. Donati, S. C. Glotzer, and P. H. Poole, "Growing Spatial Correlations of Particle Displacements in a Simulated Liquid on Cooling toward the Glass Transition," *Physical Review Letters* **82**, 5064-5067 (1999).
10. P. S. Crider, and N. E. Israeloff, "Imaging Nanoscale Spatio-Temporal Thermal Fluctuations," *Nano Letters* **6**, 887-889 (2006).
11. B. D. Terris, J. E. Stern, D. Rugar, and H. J. Mamin, "Contact electrification using force microscopy," *Physical Review Letters* **63**, 2669-2672 (1989).
12. Y. Martin, Abraham, D.W. and Wickramasinghe, H. K. , "High-resolution capacitance measurement and potentiometry by force microscopy," *Appl. Phys. Lett.* **52**, 1103-1105 (1988).
13. P. S. Crider, M. R. Majewski, J. Zhang, H. Oukris, and N. E. Israeloff, "Local dielectric spectroscopy of polymer films," to be published (2007).
14. L. E. Walther, N. E. Israeloff, E. V. Russell, and H. A. Gomariz, "Mesoscopic-scale dielectric relaxation at the glass transition," *Physical Review B (Condensed Matter and Materials Physics)* **57**, R15112-R15115 (1998).
15. H. E. Castillo, C. Chamon, L. F. Cugliandolo, J. L. Iguain, and M. P. Kennett, "Spatially heterogeneous ages in glassy systems," *Physical Review B (Condensed Matter and Materials Physics)* **68**, 134442-134441 (2003).